TECHNICAL PAPER

Numerical assessment of mixing performance for a Cross-mixer

Sak Jie Tan[1] · Kok Hwa Yu[1] · Chiang Juay Teo[2] · Boo Cheong Khoo[2]

Abstract
The present study performs a systematic investigation on the mixing performance of a Cross-mixer under the influence of relevant factors like channel inlet aspect ratio, side inlet angle, and Reynolds number. For all the flow conditions investigated, Cross-mixer yields superior mixing efficiencies, in comparison to both conventional T-mixer and Y-mixer. By employing a Cross-mixer, the mixing length can be shortened to just one-quarter of the length needed by a T-mixer, to achieve a similar mixing performance. It is also recommended that wider side inlets be employed to yield a more favorable mixing performance with reduced pressure loss. Apart from having perpendicular side inlets, side inlets with $\theta = 45°$ would yield slightly better mixing efficiency. Moreover, within the practical range of applicable Reynolds number, i.e., $0.1 \leq \mathrm{Re} \leq 10$, a Cross-mixer would consistently yield superior mixing performance over conventional mixers.

Keywords Microfluidic mixing · Mixing efficiency · Passive mixer · Side inlet

List of Symbols

AR	Aspect ratio
c	Species concentration (mol/m^3)
D	Diffusivity (m^2/s)
E	Side inlet width (m)
H	Mixing channel width (m)
$L_{M=99\%}$	Mixing length (m)
M	Mixing efficiency
P	Pressure (Pa)
U_{avg}	Average velocity (m/s)
$\boldsymbol{u}$	Velocity vector (m/s)
x	Axial direction (m)
y	Transverse direction (m)

Greek symbols

θ	Angle of side inlets (°)
μ	Dynamic viscosity (kg/ms)
ρ	Density (kg/m^3)

✉ Kok Hwa Yu
   yukokhwa@usm.my

1 School of Mechanical Engineering, Universiti Sains Malaysia, Engineering Campus, 14300 Penang, Malaysia

2 Department of Mechanical Engineering, National University of Singapore, 9 Engineering Drive 1, Singapore 117576, Singapore

1 Introduction

Research on microfluidics technology has been rapidly growing, peculiarly for chemical, biological, and biomedical applications [1, 2]. In these applications, liquid–liquid mixing is an important process for blending. In recent years, researchers have made numerous efforts to improve the performance of micromixers. The recent development of micromixers is focused on attaining an efficient mixing device with good precision control, low reactants, low sample consumption, and rapid response time [3–5]. To achieve this goal, it is pivotal to overcome the bottleneck issue, which lies in the mixing process that is often extremely slow in small microscale devices. As micromixers are generally in the scale of microns, the fluid flow at such a low Reynolds number in a microchannel is hence predominately governed by molecular diffusion. Thus, the flow is typically under laminar flow condition, creating uniform flow streams that are not conducive to fluid mixing. Under such a condition, an extended mixing channel length is thus necessary to achieve a proper mixing [6].

As commonly known, micromixers are employed to mix two or more fluids, streamed from different inlets, and then blend them in the mixing channel. Many research works have been reported pertaining to mixing enhancements for microfluidic applications [7–11]. Mixing mechanisms in micromixers can be broadly categorized into two classes, i.e., active mixers and passive mixers, in reducing the mixing length required. For active mixers, an external energy source

such as thermal mixing enhancement, periodic fluid pulsation, acoustic mixing, and electrokinetic mixing enhancement are used to enhance mixing performance. Conversely, a passive mixer requires no external energy to promote the mixing process. There are various methods proposed, including the alteration of channel structure and placing obstacles, in the attempt to generate chaotic flow in the channel to enhance the mixing performance [12, 13]. For instance, Lv et al. [9, 10, 14] presented a micromixer design with Cantor structure which is reported to significantly improve the mixing performance. Arising from its compactness, low cost and the ease of integration as compared with active micromixers, passive micromixers have been widely studied [15].

In recent years, many innovative designs of mixers were proposed. Various shapes of obstacles and channels can be employed to induce flow disturbances in enhancing the mixing efficiency. Solehati et al. [16] studied a wavy design of a microchannel that produces secondary flow in the mixing channel. It was demonstrated that a wavy microchannel could lead to chaotic flow, thereby yielding superior mixing performance indices. Rahimi et al. [17] examined the influence of channel confluence angle on the mixing performance in an asymmetrical shaped microchannel. It was reported that the mixing effectiveness increases with the rise in the flow rate ratio as well as with the drop in the confluence angle [17]. In recent years, a significant amount of research works explored the influence of obstacles on mixing efficiency, utilizing novel techniques [8, 18–21]. Recently, genetic algorithm is applied on mixer with Cantor fractal obstacles to gain an optimal mixing performance of the mixer [8]. In another recent work, it is suggested that, by employing an obstacle with a flexible vortex generator (a hybrid of active and passive mixers), it could further enhance the mixing performance [21]. In these augmented designs, the mixing fluid enhancement is accompanied by a higher pumping power required.

Apart from the augmented features on the mixing channel, the design of channel inlets is also essential in improving the mixing efficiency. The most common and simplest types of passive micromixers are the T-mixer and the Y-mixer. These mixers are commonly employed to yield insights on fluid mixing at microscale. For these basic mixers, the mixing length, employed to indicate the mixing performance, can be significantly longer. As proposed by Tan et al. [22], this mixing length can be correctly predicted for a given Péclet number at a specific mixing index of interest. Apart from having T shape and Y shape mixer inlet, the influences of different types of the microfluidic junction on mixing performance have been studied by Sarkar et al. [23]. It is reported that for many conventional mixers, the increase in mixing length is subjected to mixer aspect ratio and fluid speed. Despite being widely applied, the conventional T-mixer and Y-mixer yield relatively poor mixing performance, owing to the fact that the two streams are less distorted in symmetric junctions along the mixing channel [23]. Apart from the T-mixer and the Y-mixer, cross-channel structures with side inlets can be employed. This configuration has been employed by Abbas et al. [24], where an external Braille pin actuator array is mounted at the side inlets, while liquid flows in the main microchannel. In some of the recent works, side inlets are employed to channel the mixing fluids. Comparison of mixing performance for rectangular mixing channel with one side inlet and double side inlets were studied by Ansari et al. [25]. Cross-mixers with augmented features, like ellipse-like micropillars [26] and shifted trapezoidal blades [27], are used to investigate the mixing performance. Apart from liquid mixing, Cross-shaped channel has been employed for microdroplet generation in microfluidics [28, 29].

It is understood from the above literature review that micromixers could be enhanced using various novel designs. One of the prime features that could help promote liquid mixing is the channel inlet design. Different inlet designs like T-shape, Y-shape, Cross-shape, and other applicable shapes could help realign the fluid stream for mixing purposes. Despite the use of cross-inlets on some micromixers, to the best of our knowledge, none of the works of literature performed a systematic investigation on the use of side inlets in reorienting the mixing flow. Assessment of the geometrical variations of the side inlets on the mixing performance and its comparison with conventional T-mixer and Y-mixer are thus absent. In terms of mixing length, there has not been any quantitative comparison of these mixers. Hence, this study intends to shed some light on the direct influence of the Cross-mixer on the mixing efficiency and the mixing length. The mixing performance shall be compared with both conventional mixers to indicate the mixing benefits of the augmented inlet design. The insights gained from this study shall be useful in capitalizing on the usage of Cross-mixer to obtain better mixing performance.

2 Methodology

Figure 1 depicts the schematic of a Cross-mixer, which comprises three inlets, i.e., one main inlet (Inlet A) and two side inlets (Inlet B). Fluid A and Fluid B were forced to flow into a mixing channel using Inlet A and Inlet B, respectively. Fluid A with a relative species concentration $c^* = c/c_0$ of 1 flows through the main inlet, while Fluid B with $c^* = 0$ flows through both side inlets. The initial species concentration in Fluid A is denoted by c_0. In this study, the density of both fluids is assumed to be the same. The transverse length of the mixing channel is taken to be H, consistent with that of the main channel inlet. Meanwhile, the width of both side inlets is taken to be E which can be determined via $E = AR \times H$, where AR is the channel inlet aspect ratio (i.e., the ratio of

Fig. 1 Schematic diagram for Cross-mixer
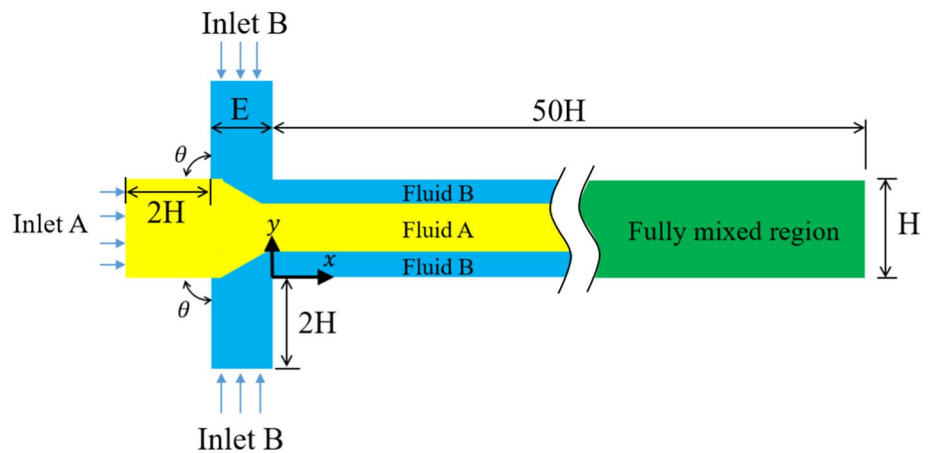
side inlet width over main inlet width). The intersection angle between the mixing channel wall and the side inlet is denoted as θ. Unless mentioned otherwise, $\theta = 90°$ is employed. For all three channel inlets, the lengths of these inlets are fixed at $2H$. In this study, a mixing channel length of $50H$ is employed, which is deemed long enough to have fully mixed fluids in the mixing channel for all the flow scenarios considered. The $x-$ and $y-$ direction represent axial and transverse directions, respectively.

In this study, Fluid A and Fluid B are taken to be incompressible Newtonian fluids. No-slip condition is employed along the channel walls, and fluids flow through the mixer under laminar flow condition. The continuity and Navier–Stokes equations of a fluid mixture are represented as follows:

$$\nabla.\mathbf{u} = 0, \tag{1}$$

$$\rho(\mathbf{u}.\nabla)\mathbf{u} = -\nabla P + \mu\nabla^2\mathbf{u}, \tag{2}$$

where ρ, μ, P, and $\mathbf{u}$ are the density of the fluid mixture (kg/m^3), the dynamic viscosity (kg /ms), the pressure field (Pa), and velocity field (m/s), respectively. The mass transport of the mixing fluid is governed by the advection–diffusion equation, which is formulated as follows:

$$\mathbf{u}.(\nabla c) = D\nabla^2 c, \tag{3}$$

where c is the species concentration (mol/m^3) and D is the diffusivity (m^2/s). It is also worth noting that the present study does not considered any chemical reaction. In this study, Fluid A and Fluid B are forced at the channel inlets with uniform flow velocity. The same flow rate is enforced on Fluid A and Fluid B. The Reynolds number $\left(\mathrm{Re} = \rho U_{\mathrm{avg}}H/\mu\right)$ is defined based on the average flow velocity U_{avg} attained through the mixing channel. Meanwhile, pressure outlet condition is imposed at the channel outlet. The Schmidt number of the fluid is given by $\mathrm{Sc} = \mu/\rho D$. In this study, the Schmidt number is fixed at $\mathrm{Sc} = 100$.

In this study, a two-dimensional, steady, incompressible laminar flow model is employed. SIMPLE (Semi Implicit Method for Pressure Linked Equations) method is employed to solve the pressure–velocity coupling. The numerical solution for pressure is based on second-order while a second-order upwind scheme is employed for momentum and species concentration. In all the simulations performed in this study, the relative convergence criteria of 10^{-10} are employed for continuity, momentum, and advection–diffusion equations. ANSYS FLUENT 19.2 is employed to solve the mixing flow problem, governed by Eqs. (1) - (3), along with the boundary conditions stated.

The species concentration fields attained from numerical solution are then further analyzed to assess the resulting mixing efficiency. At a specific axial position along the mixing channel, the local mixing performance is given as

$$M_{\mathrm{x}} = \left[1 - 2\sqrt{\frac{\int_0^H (c^* - 0.5)^2 dy}{\int_0^H dy}}\right]_x \times 100\% \, . \tag{4}$$

Using Eq. (4), it should be noted that the value of M varies from 0 to 100%. When $M = 0\%$ is attained, it indicates an entirely unmixed state. Meanwhile, $M = 100\%$ indicates a complete mixing. In addition to mixing efficiency, another mixing performance based on mixing length $\left(L_{\mathrm{M=99\%}}\right)$ is assessed. This length is measured based on the axial length required from the entrance of the mixing channel (i.e., $x/H = 0$) to reach 99% mixing efficiency.

3 Result and discussion

3.1 Grid independence and validation

To establish an optimal grid resolution for this study, a grid independence test is first performed. A total of four grid resolutions were considered. The number of elements used

are 39200, 61250, 88200, and 120050. A uniform grid is used to mesh the flow region of a Cross-mixer. The mixing flow at Re = 1 and Sc = 100 is simulated. This mixing flow scenario can be realized in the practical condition using a working fluid with density of 1000kg/m^3, dynamic viscosity of 1×10^{-3}kg/ms, and diffusivity of 1×10^{-8}m^2/s. With mixing channel width of 1×10^{-4}m, mixing flow with Re = 1 can be attained using an average flow velocity of 0.01m/s in the mixing channel. For this grid independence test, a Cross-mixer with inlet *AR* (a ratio of side inlet width over main inlet width) of 0.5 is employed. The width of each side inlet is thus 0.5H. To maintain the flow rate desired, inlet velocity of 0.005m/s is applied at both Inlet A and Inlet B. Using these grid resolutions, the relative species concentration (c^*) profiles along channel width at $x/H = 1$ are illustrated in Fig. 2. As shown, it can be clearly observed that the relative species concentration (c^*) profiles, yielded by different grid resolutions, are all in good agreement. The resulting mixing efficiency is tabulated in Table 1. As stated in this table, numerical simulation using 88200 elements yields mixing efficiency of 47.57%. By increasing the number of elements to 120 050, this would only result in 0.07% deviation in the mixing efficiency. Thus, this study employs a numerical model that uses approximately 88200 elements to investigate the influence of relevant factors on the mixing performance of a Cross-mixer.

Using the mentioned grid resolution and numerical model, validation of numerical result is then benchmarked with existing experimental data presented by Lee et al. [30], which is performed in a conventional T-mixer with 2 cm long mixing channel and 200 microns channel width. The mixing flow simulated is at Re$_{D_H}$ = 8 with Sc = 1000. As depicted in Fig. 3, a comparison of relative species concentration
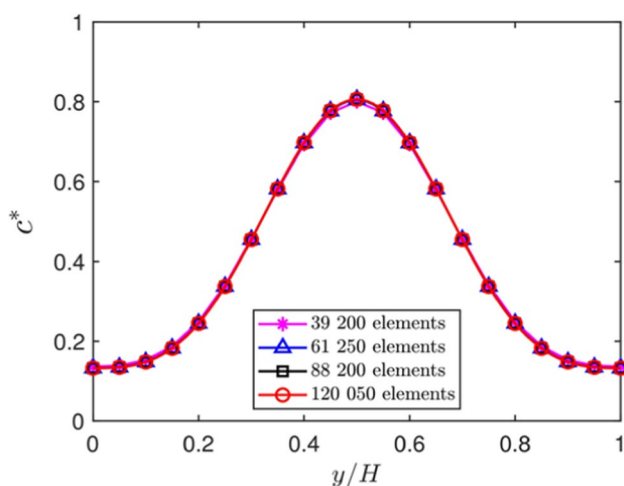
Table 1 Convergence study on mixing efficiency performance

Mesh	Number of elements	$M_{1H}(\%)$	Absolute percentage deviation (%)
1	39 200	48.68	2.40
2	61 250	47.70	0.35
3	88 200	47.57	0.07
4	120 050	47.53	Baseline

(c^*) profile along the channel width is shown at $x/H = 50$. Owing to the good accuracy attained for numerical results, in comparison to the data presented by Lee et al. [30], this thus ascertains the validity of the present numerical model.

3.2 Comparison with conventional T-mixer and Y-mixer

Channel inlet design is deemed to play a principal role in enhancing the mixing performance. To assess the mixing performance of the Cross-mixer, comparisons with other conventional mixers, i.e., T-mixer and Y-mixer, are performed. For this comparison, simulations with the same flow scenario (with Re = 1 and Sc = 100) are enforced. Cross-mixer with channel inlets aspect ratio *AR* of 0.5 is employed for this comparison. Meanwhile, for the Y-mixer, the intersection angle between two inlets is fixed at 60$^{\circ 0}$. Regardless of the channel inlet designs employed, the combined channel width for Inlet B has the same width as that of Inlet A. Specifically for the T-mixer and the Y-mixer used, the width of channel inlets is all fixed with length H. To attain mixing flow of Re = 1, inlet velocity of 0.005m/s is applied at all channel inlets, regardless of the channel inlet designs. This
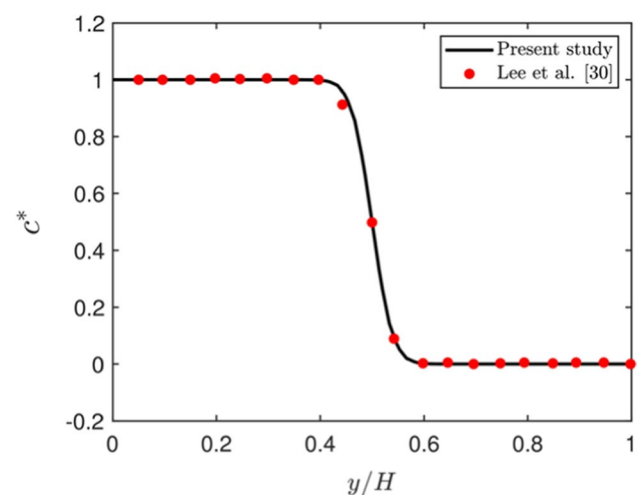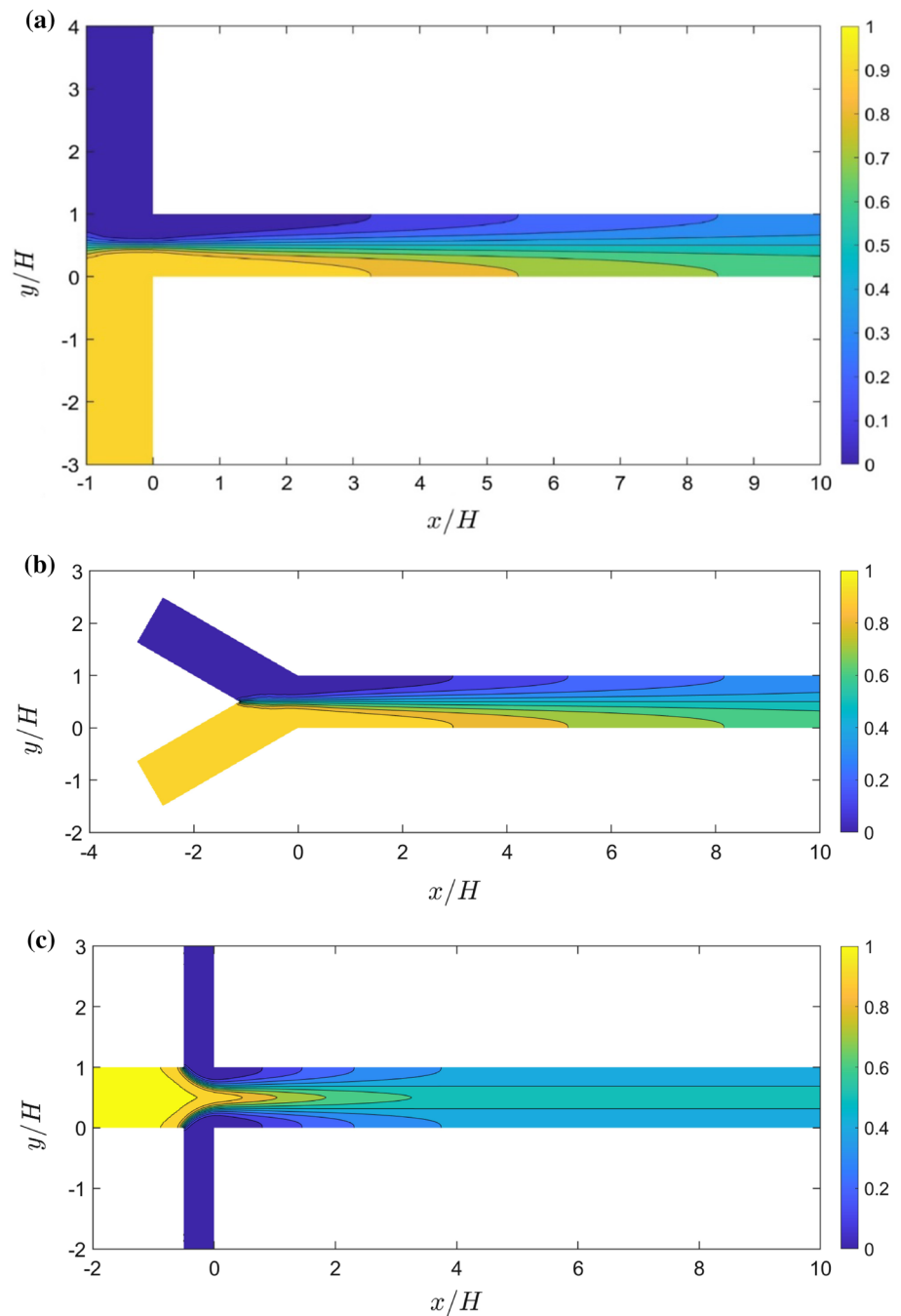

Fig. 2 Relative species concentration along channel width (y/H) at axial position of $x/H = 1$ with mixing flow at Re = 1 using different number of elements

Fig. 3 Relative species concentration along channel width (y/H) at axial position of $x/H = 50$, as compared with Lee et al. [30]

will give rise to the average fluid velocity of 0.01m/s in the mixing channel.

Figure 4 shows the relative species concentration distributions for different mixers along the mixing channel. As can be clearly seen from this figure, the Cross-mixer yields low c^* value near to both channel walls (where $y/H \to 0$ and 1). Based on the relative species concentration distribution, the c^* profiles are plotted at two different axial positions (i.e., $x/H = 1$ and $x/H = 10$), as illustrated in Fig. 5. Unlike that of a T-mixer and a Y-mixer, the species concentration profile along the channel width for a Cross-mixer

is symmetric about the flow centerline (at $y/H = 0.5$). The symmetric distribution is arising from the two side inlets design of the Cross-mixer, thus exhibiting a balanced c^* distribution for both halves of the mixing channel. For a T-mixer and a Y-mixer, the species concentration exhibits an anti-symmetric pattern with $c^* > 0.5$ for $y/H < 0.5$, and $c^* < 0.5$ for $y/H > 0.5$. The different species concentration on both halves of the channel is also reported in other existing studies [12, 31]. It is also worth highlighting that, using a Cross-mixer, $c^* \to 0.5$ is observed at $x/H = 10$, indicating an almost complete mixing condition. This is indeed a stark

Fig. 4 Relative species concentration (c^*) field for mixing flow for different junction mixers, i.e., **a** T-mixer, **b** Y-mixer, and **c** Cross-mixer
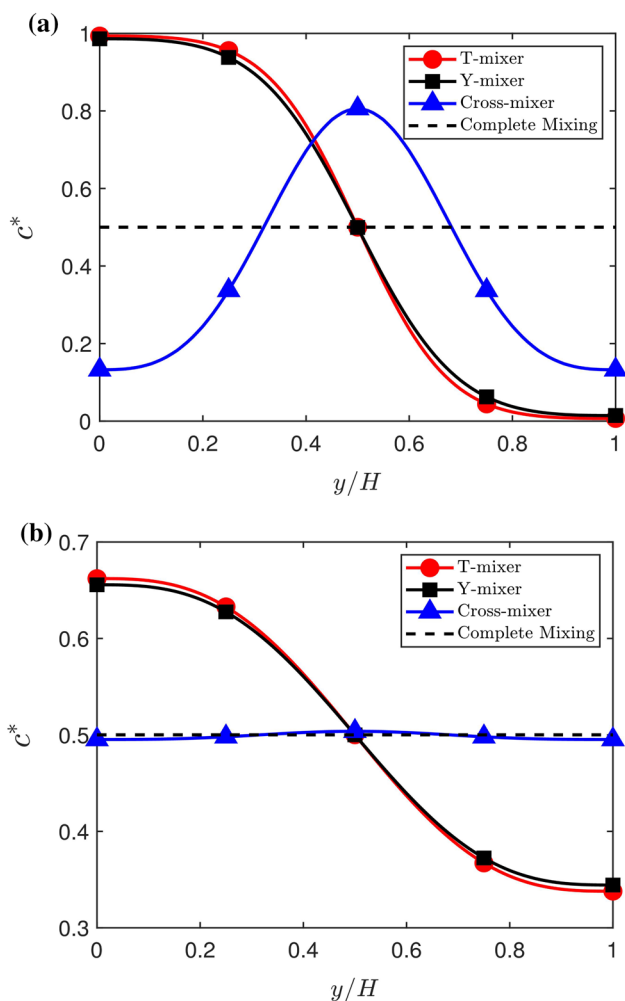
(a)

(b)

Fig. 5 The c^* profile for mixing flow in different liquid mixers at **a** $x/H = 1$, and **b** $x/H = 10$, with Reynolds number being fixed at Re = 1

Table 2 Comparison of mixing efficiency for T-mixer, Y-mixer, and Cross-mixer at Re = 1 at the axial locations of $x/H = 1, 10,$ and 20

Type of mixer	$M_{1H}(\%)$	$M_{10H}(\%)$	$M_{20H}(\%)$	$\Delta P/L(\text{Pa/m})$
T-mixer	18.33	75.15	93.64	12 126
Y-mixer	21.00	76.14	93.89	12 027
Cross-mixer	47.57	99.33	99.99	12 345

was attained in close proximity to the mixing channel entrance, i.e., at $x/H = 1$, with more than 150% increase in mixing efficiency over that of a T-mixer. Based on the mixing efficiencies along the axial direction, the mixing efficiency distribution along the mixing channel is plotted in Fig. 6. The computed $L_{M=99\%}$ for the Cross-mixer and the conventional T-mixer are 9.2 and 33.6H, respectively. This implies that a significant reduction in mixing length can be attained by using the Cross-mixer. In other words, under the same flow condition, well-mixed fluid can be achieved with a shorter channel length using a Cross-mixer. As compared with the conventional T-mixer, the Cross-mixer would yield a 72.6% reduction in terms of $L_{M=99\%}$. This suggests that the mixing channel length of a Cross-mixer can be shortened to just one-quarter of the channel length needed by a T-mixer, to achieve the same mixing efficiency. This enormous mixing enhancement attained by a Cross-mixer is accompanied by a negligible increase in pressure drop, as shown in Table 2. The pressure gradient is measured based on the differential pressure between that at channel inlets and that at the mixing channel outlet (i.e., $x/H = 50$).
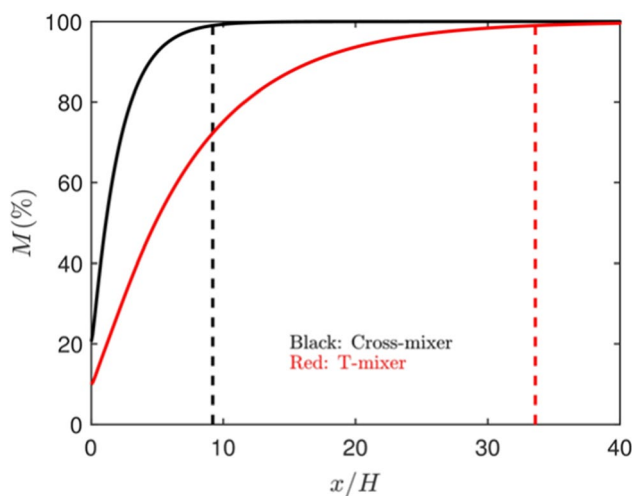
contrast with the relative species concentration exhibited by conventional T-mixer and Y-mixer which still possesses unmixed region in both halves of the mixing channel. Poor mixing performance yielded by both T-mixer and Y-mixer are owing to the two distinct streams formed. As the liquid mixing in conventional mixers is mainly driven by transverse molecular diffusion, this hinders rapid mixing of liquids. For a Cross-mixer, with side inlets, three distinct streams are formed in the mixing channel, allowing swift mixing at both halves of the channel.

To further assess the mixing performance of these mixers, the mixing efficiency (M) at different axial locations are tabulated in Table 2. The computed mixing performances show significant mixing enhancement for a Cross-mixer. For all the three axial positions examined at $x/H = 1, 10,$ and 20, the mixing efficiencies for a Cross-mixer are better than that of the conventional T-mixer and Y-mixer. The greatest percentage of improvement

Fig. 6 Distribution of mixing efficiency along axial direction for Cross-mixer and T-mixer at Re = 1 and Sc = 100. The dashed lines correspond to the locations of $L_{M=99\%}$

3.3 Effect of channel inlet aspect ratio

The ratio of side inlet width over main inlet width (denoted as inlet AR) was also found to exert significant influence on the mixing performance for a Cross-mixer. Five different values of inlet AR are studied, ranging from 0.125 to 2. Despite the change of inlet AR value, the width of the main inlet is kept constant at H. At largest inlet AR value of 2, both side inlets are twice wider than the main inlet. In the case where a Cross-mixer with mixing channel width of 1×10^{-4}m is employed, this will yield side inlet channel width of 2×10^{-4}m. For this particular Cross-mixer, inlet velocity of 0.00125m/s is enforced at the side inlets (i.e., Inlet B). Maintaining the same flow rate through Inlet A and Inlet B, Fluid A is forced with an inlet velocity of 0.005m/s through Inlet A. This produces fluid flow of Re = 1 in the mixing channel. Figure 7 shows the relative species concentration distribution for flow scenarios with inlet AR of 0.25 and 1. Despite different side inlet widths employed, the resulted c^* profiles are deemed to be almost identical. Using the relative species concentration distribution attained, the c^* profiles along the channel width at $x/H = 1$ and $x/H = 10$ are plotted in Fig. 8. The c^* profiles obtained are qualitatively similar, with lower c^* value in the vicinity of both channel walls (i.e., $y/H = 0$ and 1), while peak value of c^* at the flow centerline (i.e., $y/H = 0.5$). Quantitatively, the c^* distribution along the channel width offsets toward 0.5, as the inlet AR value increases. This trend is consistent along the axial direction, as shown in Fig. 8a and b for two different axial positions. In terms of mixing efficiency, as expected, the M value is consistently higher for flow scenarios with larger inlet AR value. At $x/H = 1$, the mixing efficiency for inlet AR of 2 is nearly 30% higher than that for inlet AR of 0.125. This implies that wider side inlets are more favorable for mixing purposes. With wider side inlets, a larger side flow entrance area tends to promote better mixing. As the mass flow rate through the mixing channel is maintained, the size of the side inlet width would determine the velocity of Fluid B entering the channel. As the mass flow rate is maintained in this study, smaller side inlet width shall yield higher flow speed from the side inlets and vice versa. With higher flow speed through narrow side inlets, the pressure drop is significantly higher as shown in Table 3. The pressure drop ($\Delta P/L$) for the case with inlet AR of 0.125 is found to be more than twice higher than that of inlet AR of 2. In short, having wider side inlets, this would not only yield better mixing performance but would also require lesser pumping power.

Fig. 7 Relative species concentration (c^*) field for mixing flow with (a) inlet AR of 0.25, and (b) inlet AR of 1
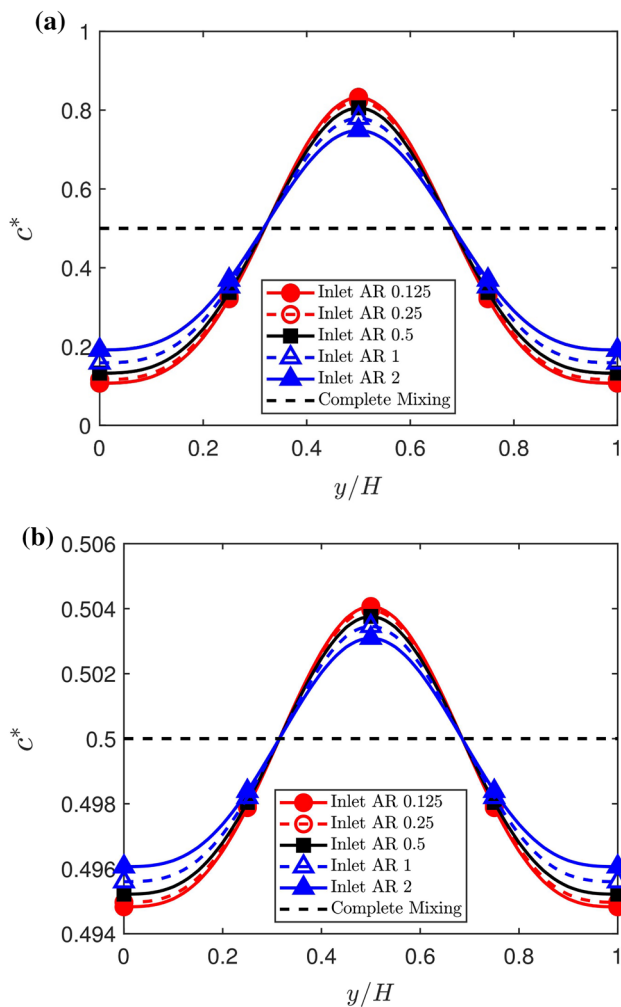
(a)

(b)
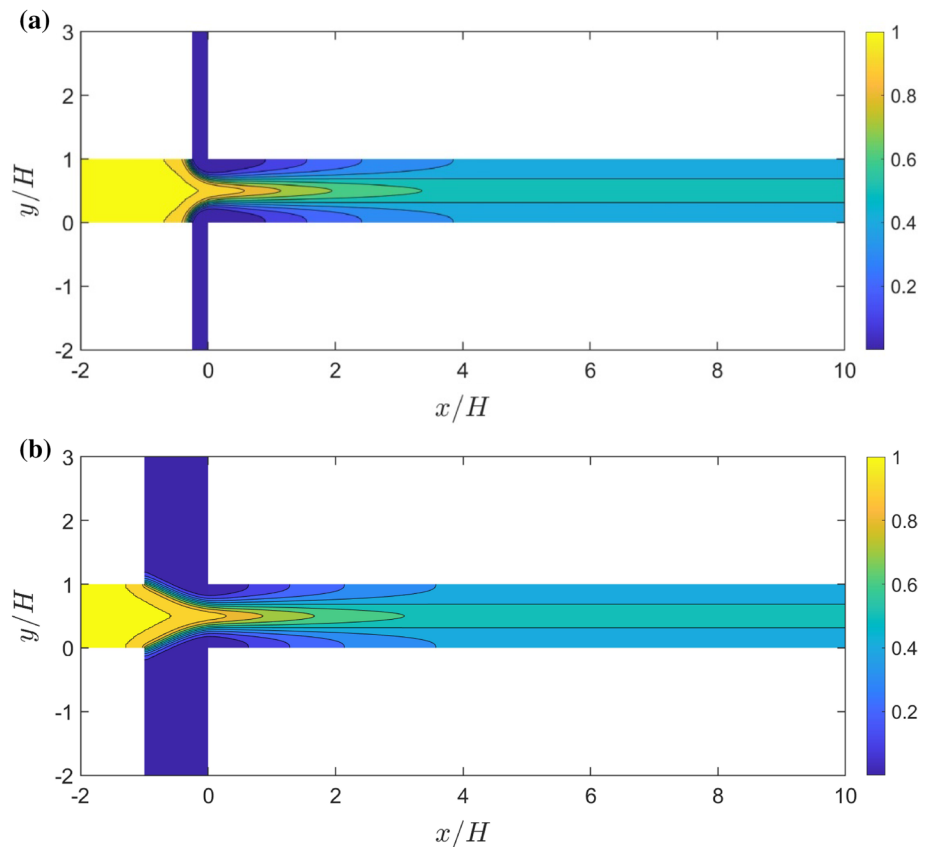
Fig. 8 The c^* profile at **a** $x/H = 1$ and **b** $x/H = 10$ with Re = 1 for mixing flow on different inlet aspect ratios

Table 3 Comparison of mixing efficiency for Cross-mixer with different inlet AR values, at Re = 1

Inlet AR	$M_{1H}(\%)$	$M_{10H}(\%)$	$\Delta P/L$(Pa/m)
0.125	43.51	99.28	23 648.08
0.25	44.96	99.30	14 473.72
0.5	47.57	99.33	12 345.2
1	51.63	99.39	11 865.4
2	56.55	99.45	11 733.1

3.4 Effect of angle of side inlets

The effect arising from the angle of side inlets is also studied, in the attempt to explore further enhancement in the mixing performance. The angles, consisting of θ of $45, 90,$ and $135°$, are investigated. Figure 9 depicts the c^* distributions for flow scenarios with different side inlet angles. It is worth noting

that uniform inlet velocity is employed at the inlets, similar to that prescribed earlier. For side inlets with $\theta = 90°$, Fluid B is forced into the mixing channel perpendicularly. For $\theta = 45°$, the entrance of the side inlets are directed toward the downstream direction while it is pointed toward the upstream direction for $\theta = 135°$. Based on numerical results attained, the c^* fields in the mixing channel are identical similar, regardless of different θ used. The respective c^* profiles at $x/H = 1$ at Re = 1 are depicted in Fig. 10. The resulting mixing efficiencies are shown in Table 4. Among the side inlet angles studied, $\theta = 45°$ is found to yield slightly better mixing efficiency. At $x/H = 1$, $M = 51.04\%$ can be attained using a Cross-mixer with $\theta = 45°$, which is 5.7% higher as compared with that of $\theta = 135°$. The mixing enhancement tends to subdue in the downstream. In accordance with existing studies on Y-mixers, having inlets inclined toward mixing channel could elevate the mixing performance, as compared with that of the T-mixer [12, 17]. In addition to the enhancement of the mixing efficiency, the pressure loss is also slightly reduced using the same design.

3.5 Effect of Reynolds number

Apart from geometrical effects, mixing performance is also dependent on the flow Reynolds number [12]. The Reynolds number investigated is bounded between 0.1 and 10, corresponding to fluid speed in the range between 0.001 and 0.1m/s in the mixing channel, respectively. It should be noted that a Cross-mixer with inlet AR of 0.5 and $\theta = 90°$ is employed to study the influence of Re.

Figure 11 shows the relative species concentration profile along the channel width at $x/H = 1$. At that specific axial position, the plots indicate that, at very low Reynolds number (i.e., Re = 0.1), complete mixing could be achieved, with $c^* \sim 0.5$ along the $y-$ direction. As the flow Re is higher, the c^* profile tends to offset away from 0.5. This is arising from the fact that the fluid mixing in the spanwise direction is dominated by molecular diffusion. When Re increases, it induces a stronger axial force convection. Thus, a longer channel length is required to achieve a complete mixing and vice versa. Thus, a lower mixing efficiency is attained at the specific position as compared with the results for low Re. The dependency of mixing efficiency on Reynolds number at fixed axial positions (i.e., $x/H = 1$ and $x/H = 10$) are depicted in Fig. 12. As expected, the mixing efficiency at a fixed x position is higher for mixing flow at low Re. As Re increases, M gradually decreases. Comparing both the T-mixer and the Cross-mixer, the latter yields better mixing efficiency than the former. For Re = 10, at $x/H = 10$, the Cross-mixer could yield 39.8% mixing efficiency, while T-mixer would only produce 15.1% at the same location. The mixing efficiency is almost double that yielded by a T-mixer. As anticipated, in terms of mixing length, a shorter $L_{M=99\%}$ is required to attain

Fig. 9 Relative species concentration (c^*) field at Re = 1 for mixing flow with different inlet angles of side inlets
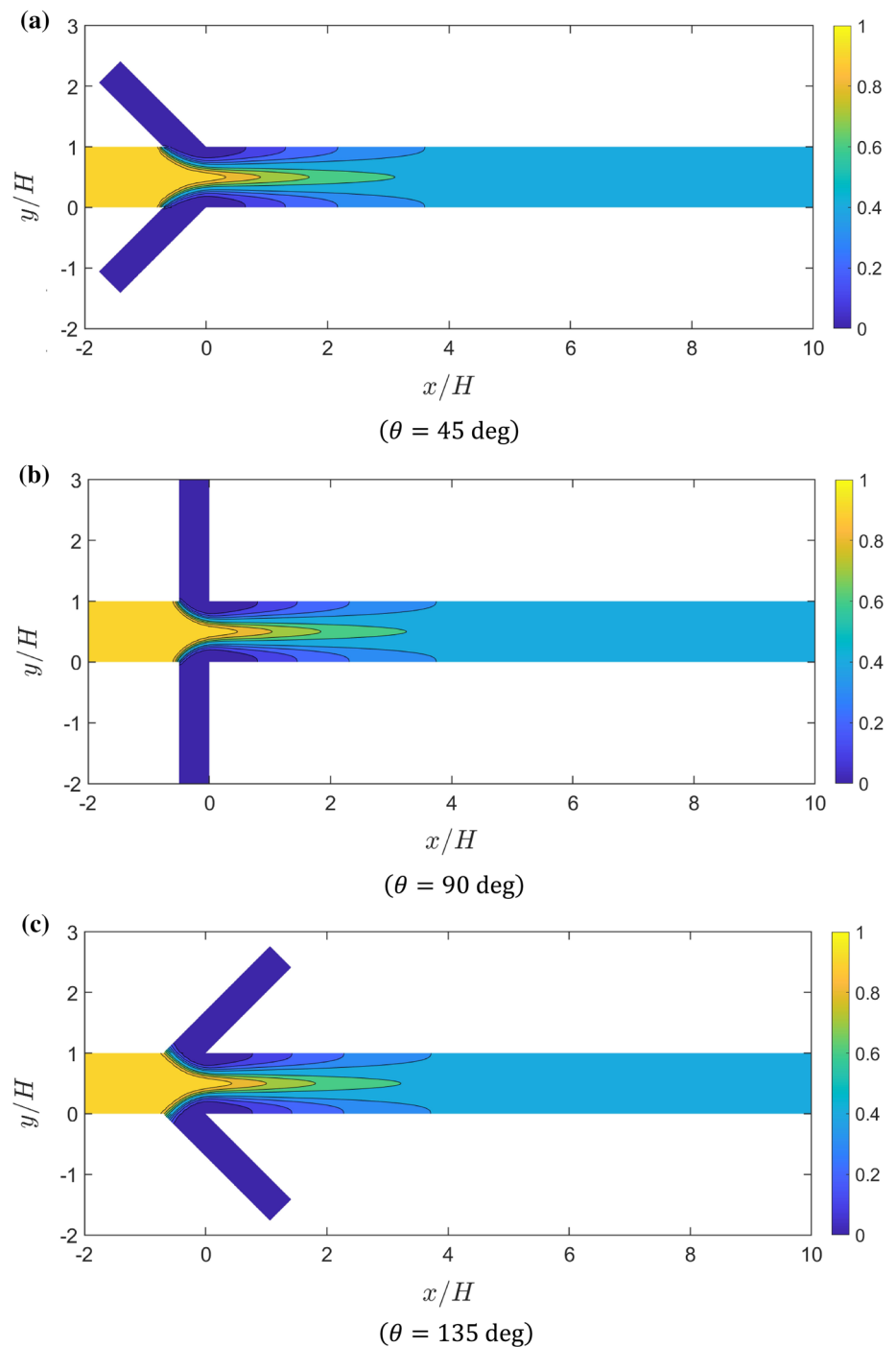
fully mixed fluid for a Cross-mixer. This is clearly shown in Fig. 13 for flow scenarios with Re between 0.1 and 1. For Re > 1, the $L_{M=99\%}$ needed for T-mixer, exceeded the mixing channel length of $50H$ simulated in this study. As indicated earlier, the mixing length required by a Cross-mixer is nearly one quarter of the channel length required by a T-mixer. This is consistent within the range of Re investigated. This implies that the mixing benefit of the Cross-mixer can be consistently attained, regardless of the flow Reynolds number. In essence, the superior mixing performance of the Cross-mixer could be extensively utilized, significantly shortening the mixing length with minimal increase in pressure drop.
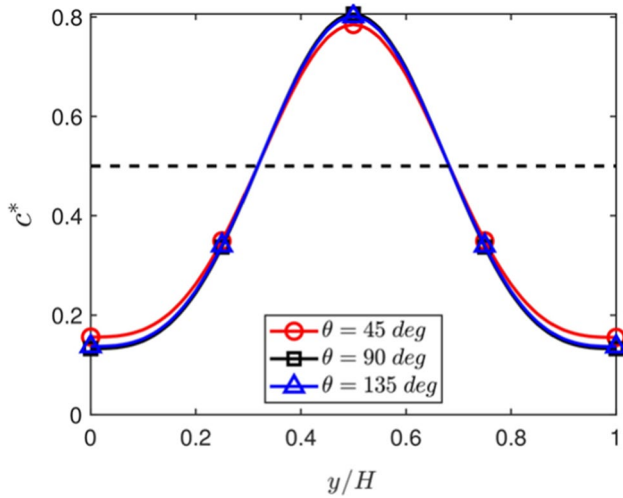
Fig. 10 The c^* profile at $x/H = 1$ with Re = 1 for mixing flow with different inlet angles of side inlets

Table 4 Comparison of mixing efficiency for Cross-mixer with different side inlet angles, at Re = 1

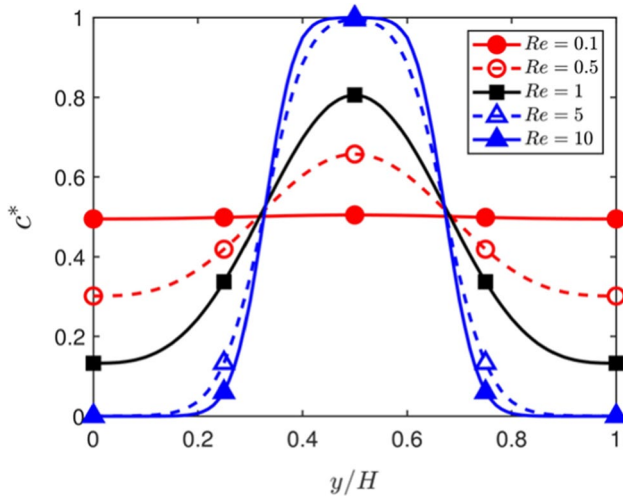| Side inlet angle (θ)	$M_{1H}(\%)$	$M_{10H}(\%)$	$\Delta P/L(Pa/m)$
45°	51.04	99.38	12 244.23
90°	47.57	99.33	12 346.15
135°	48.27	99.34	12 400.00

Fig. 11 The c^* profile at $x/H = 1$ for mixing flow at different Reynolds numbers using a Cross-mixer with angle 90 degrees
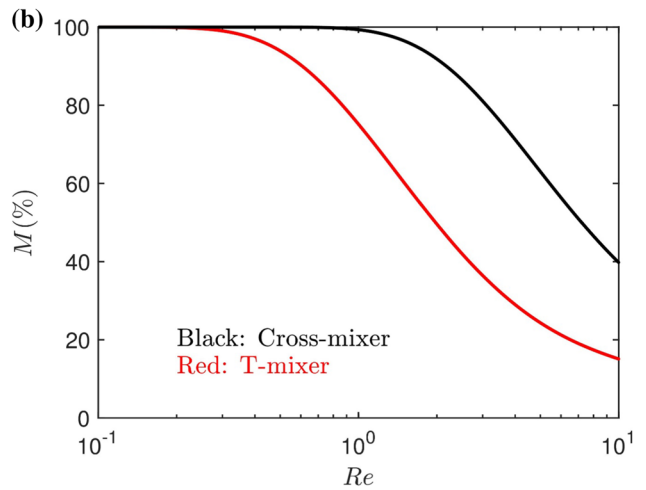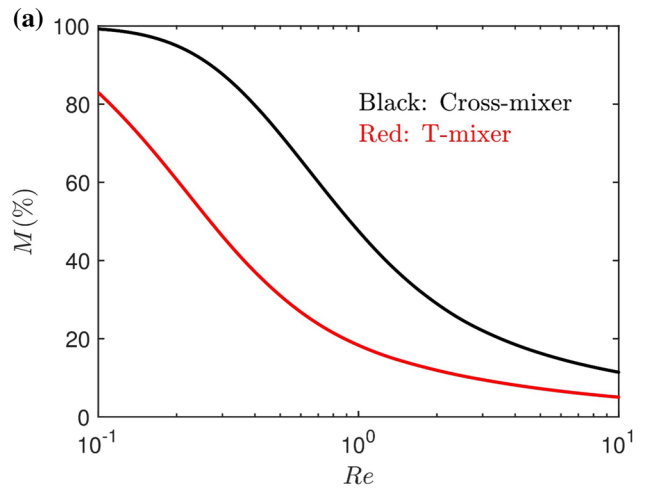

Fig. 12 Variation of mixing efficiency with flow Reynolds number, at **a** $x/H = 1$, and **b** $x/H = 10$ for Cross-mixer and T-mixer
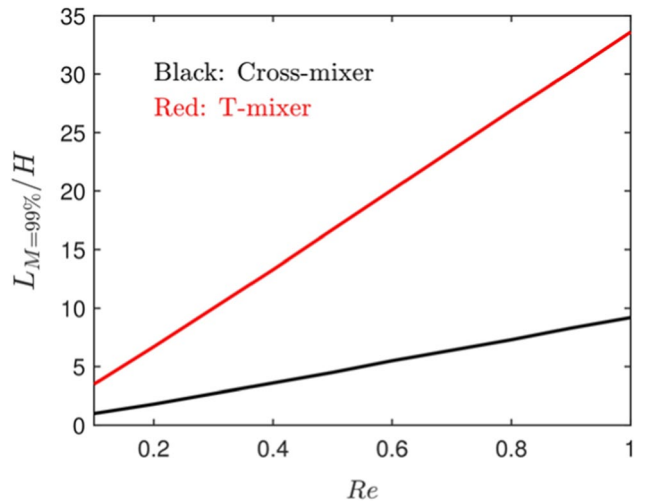

Fig. 13 Variation of normalized mixing length $\left(L_{M=99\%}/H\right)$ with flow Reynolds number for Cross-mixer and T-mixer

4 Conclusion

In the present study, a systematic investigation on the use of side inlets to re-orientate the mixing flow is explored. A numerical study has been carried out to compare the mixing performance between a Cross-mixer and the conventional mixer designs, i.e., a T-mixer and a Y-mixer. Liquid mixing in these mixers has been numerically investigated using a two-dimensional, steady, incompressible laminar flow model. It is revealed that the Cross-mixer demonstrates superior mixing performances as compared with that of the T-mixer and the Y-mixer. At Re = 1 and Sc = 100, simulation results predicted that a Cross-mixer could gain almost complete mixing at $x/H = 10$ where channel length of only 10 times the channel width is needed. At this position, T-mixer and Y-mixer still possess unmixed regions. At any axial position, a Cross-mixer would consistently yield higher mixing efficiency value than those produced by a T-mixer and a Y-mixer. As indicated by the results on mixing length $L_{M=99\%}$, the Cross-mixer requires only one-quarter of the channel length required by a T-mixer, to achieve the same mixing efficiency. It is also found that the mixing enhancement holds within the practical range of Reynolds number for micromixer applications, i.e., $0.1 \leq Re \leq 10$. In addition, the numerical result implies that wider side inlets are more favorable for mixing purposes. The results show that the M value is consistently higher for flow scenarios with larger inlet AR value. Apart from using perpendicular side inlets, the angle of side inlets of $\theta = 45°$ is found to yield slightly better mixing efficiency. In short, it could be inferred that significant mixing enhancement could be obtained, simply by employing Cross-shape mixer design, without any augmented features in the mixing channel. With these insights, utilization of the Cross-shape mixer is envisaged to propel further development in microfluidic technology, especially for liquid mixing applications.

References

1. Rashidi S, Bafekr H, Valipour MS, Esfahani JA (2018) A review on the application, simulation, and experiment of the electrokinetic mixers. Chem Eng Process 126:108–122. https://doi.org/10.1016/j.cep.2018.02.021
2. Han W, Chen X (2020) A review: applications of ion transport in micro-nanofluidic systems based on ion concentration polarization. J Chem Technol Biotechnol 95(6):1622–1631. https://doi.org/10.1002/jctb.6288
3. Damiati S, Kompella UB, Damiati SA, Kodzius R (2018) Microfluidic devices for drug delivery systems and drug screening. Genes 9(2):103. https://doi.org/10.3390/genes9020103
4. Nguyen N-T, Hejazian M, Ooi CH, Kashaninejad N (2017) Recent advances and future perspectives on Microfluidic liquid handling. Micromachines 8(6):186. https://doi.org/10.3390/mi8060186
5. Streets AM, Huang Y (2013) Chip in a lab: microfluidics for next generation life science research. Biomicrofluidics 7(1):11302. https://doi.org/10.1063/1.4789751
6. Lee C-Y, Chang C-L, Wang Y-N, Fu L-M (2011) Microfluidic mixing: a review. Int J Mol Sci 12(5):3263–3287. https://doi.org/10.3390/ijms12053263
7. Bayareh M, Ashani MN, Usefian A (2020) Active and passive micromixers: A comprehensive review. Chem Eng Process - Process Intensif 147:107771. https://doi.org/10.1016/j.cep.2019.107771
8. Chen X, Lv H (2022) New insights into the micromixer with Cantor fractal obstacles through genetic algorithm. Sci Rep 12(1):4162. https://doi.org/10.1038/s41598-022-08144-w
9. Lv H, Chen X, Zeng X (2021) Optimization of micromixer with Cantor fractal baffle based on simulated annealing algorithm. Chaos, Solitons Fractals 148:111048. https://doi.org/10.1016/j.chaos.2021.111048
10. Lv H, Chen X, Wang X, Zeng X, Ma Y (2022) A novel study on a micromixer with Cantor fractal obstacle through grey relational analysis. Int J Heat Mass Transf 183:122159. https://doi.org/10.1016/j.ijheatmasstransfer.2021.122159
11. Lv H, Chen X (2021) New insights into the mechanism of fluid mixing in the micromixer based on alternating current electric heating with film heaters. Int J Heat Mass Transf 181:121902. https://doi.org/10.1016/j.ijheatmasstransfer.2021.121902
12. Hsieh S-S, Lin J-W, Chen J-H (2013) Mixing efficiency of Y-type micromixers with different angles. Int J Heat Fluid Flow 44:130–139. https://doi.org/10.1016/j.ijheatfluidflow.2013.05.011
13. Khaydarov V, Borovinskaya ES, Reschetilowski W (2018) Numerical and experimental investigations of a Micromixer with chicane mixing geometry. Appl Sci 8(12):2458. https://doi.org/10.3390/app8122458
14. Lv H, Chen X, Li X, Ma Y, Zhang D (2022) Finding the optimal design of a Cantor fractal-based AC electric micromixer with film heating sheet by a three-objective optimization approach. Int Commun Heat Mass Transfer 131:105867. https://doi.org/10.1016/j.icheatmasstransfer.2021.105867
15. Cai G, Xue L, Zhang H, Lin J (2017) A Review on Micromixers. Micromachines 8(9):274. https://doi.org/10.3390/mi8090274
16. Solehati N, Bae J, Sasmito AP (2014) Numerical investigation of mixing performance in microchannel T-junction with wavy structure. Comput Fluids 96:10–19. https://doi.org/10.1016/j.compfluid.2014.03.003
17. Rahimi M, Akbari M, Parsamoghadam MA, Alsairafi AA (2015) CFD study on effect of channel confluence angle on fluid flow pattern in asymmetrical shaped microchannels. Comput Chem Eng 73:172–182. https://doi.org/10.1016/j.compchemeng.2014.12.007
18. Ritter P, Osorio-Nesme A, Delgado A (2016) 3D numerical simulations of passive mixing in a microchannel with nozzle-diffuser-like obstacles. Int J Heat Mass Transf 101:1075–1085. https://doi.org/10.1016/j.ijheatmasstransfer.2016.05.035
19. Tan SJ, Yu KH, Ismail MA, Teoh YH (2020) Enhanced liquid mixing in T-mixer having staggered fins. Asia-Pac J Chem Eng 15(6):e2538. https://doi.org/10.1002/apj.2538
20. Tan SJ, Yu KH, Ismail MA, Teoh YH (2021) Numerical assessment on liquid mixing in a T-mixer containing tri-fin. Asia-Pacific J Chem Eng 6:e2703. https://doi.org/10.1002/apj.2703
21. Dadvand A, Hosseini S, Aghebatandish S, Khoo BC (2019) Enhancement of heat and mass transfer in a microchannel via

passive oscillation of a flexible vortex generator. Chem Eng Sci 207:556–580. https://doi.org/10.1016/j.ces.2019.06.045

22. Tan SJ, Yu KH, Sidhu JSS, Ismail MA (2022) Mixing length correlation for laminar liquid mixing in wall-bounded flows. Int Commun Heat Mass Transfer 132:105913. https://doi.org/10.1016/j.icheatmasstransfer.2022.105913

23. Sarkar S, Singh KK, Shankar V, Shenoy KT (2014) Numerical simulation of mixing at 1–1 and 1–2 microfluidic junctions. Chem Eng Process 85:227–240. https://doi.org/10.1016/j.cep.2014.08.010

24. Abbas Y, Miwa J, Zengerle R, Von Stetten F (2013) Active continuous-flow micromixer using an external braille pin actuator array. Micromachines 4(1):80–89. https://doi.org/10.3390/mi4010080

25. Ansari MA, Kim K-Y, Kim SM (2010) Numerical study of the effect on mixing of the position of fluid stream interfaces in a rectangular microchannel. Microsyst Technol 16(10):1757–1763. https://doi.org/10.1007/s00542-010-1100-2

26. Tran-Minh N, Dong T, Karlsen F (2014) An efficient passive planar micromixer with ellipse-like micropillars for continuous mixing of human blood. Comput Methods Programs Biomed 117(1):20–29. https://doi.org/10.1016/j.cmpb.2014.05.007

27. Le The H, Le Thanh H, Dong T, Ta BQ, Tran-Minh N, Karlsen F (2015) An effective passive micromixer with shifted trapezoidal blades using wide Reynolds number range. Chem Eng Res Des. https://doi.org/10.1016/j.cherd.2014.12.003

28. Han W, Chen X (2019) New insights into the pressure during the merged droplet formation in the squeezing time. Chem Eng Res Des 145:213–225. https://doi.org/10.1016/j.cherd.2019.03.002

29. Han W, Chen X (2021) A review on microdroplet generation in microfluidics. J Braz Soc Mech Sci Eng 43(5):247. https://doi.org/10.1007/s40430-021-02971-0

30. Lee CY, Lin C, Hung MF, Ma RH, Tsai CH, Lin CH, Fu LM (2006) Experimental and numerical investigation into mixing efficiency of micromixers with different geometric barriers. Mater Sci Forum 505–507:391–396. https://doi.org/10.4028/www.scientific.net/MSF.505-507.391

31. Tserepi A, Gogolides E, Tsougeni K, Constantoudis V, Valamontes ES (2005) Tailoring the surface topography and wetting properties of oxygen-plasma treated polydimethylsiloxane. J Appl Phys 98(11):113502. https://doi.org/10.1063/1.2136421